EARTH SURFACE PROCESSES AND LANDFORMS
Earth Surf. Process. Landforms **41**, 499–512 (2016)

Published online 14 October 2015 in Wiley Online Library
(wileyonlinelibrary.com) DOI: 10.1002/esp.3840

Sources of dissolved silica to the fjords of northern Patagonia (44–48°S): the importance of volcanic ash soil distribution and weathering

Elke Vandekerkhove,[1]* Sébastien Bertrand,[1] Brian Reid,[2] Astrid Bartels[1] and Bernard Charlier[3]
[1] Renard Centre of Marine Geology, Ghent University, Krijgslaan 281 S8, 9000 Gent, Belgium
[2] Centro de Investigación en Ecosistemas de la Patagonia, Universidad Austral de Chile, Francisco Bilbao 323, Coyhaique, Chile
[3] Department of Geology, University of Liège, 4000 Sart Tilman, Belgium

Received 27 April 2015; Revised 4 September 2015; Accepted 7 September 2015

*Correspondence to: Elke Vandekerkhove, Renard Centre of Marine Geology, Ghent University, Krijgslaan 281 S8, 9000 Gent, Belgium. E-mail: elke.vandekerkhove@ugent.be

ESPL
Earth Surface Processes and Landforms

ABSTRACT: Dissolved silica (DSi) plays an important biogeochemical role in the fjords of northern Chilean Patagonia (44–48°S), where it drives high biogenic productivity and promotes carbon burial. It is generally believed that the DSi riverine input to lakes and coastal environments is controlled by a combination of factors including lithology, climate, topography, vegetation, and meltwater input. In northern Chilean Patagonia several authors have proposed that the postglacial volcanic ash soils (andosols) may play a significant role in the high supply of DSi to the regional fjords. To assess the influence of andosols on DSi concentrations in north Patagonian rivers, we mapped andosol thickness and compared our results with river chemistry. The mineralogical and geochemical composition of three representative andosol profiles was also examined to evaluate the efficiency of weathering processes. The andosol thickness map clearly demonstrates that volcanic ash was predominantly deposited on the eastern side of the regional volcanoes, reflecting the influence of the prevailing westerly winds on the distribution of pyroclastic material. Mineralogical and geochemical results show that the andosol parent material has the typical andesitic basaltic signature of the regional volcanoes, i.e. high amounts of amorphous material, plagioclase, K-feldspar, and pyroxene. Down-profile variations in soil mineralogy and geochemistry indicate increased leaching of silica with depth, resulting from weathering of the volcanic parent material. For the five studied watersheds, a highly positive correlation (R^2=0.98) was found between average andosol thickness and DSi concentrations, suggesting that andosol thickness is the main parameter affecting DSi concentrations in north Patagonian river systems. On seasonal timescales, increased precipitation (winter) and glacial meltwater (summer) input can significantly reduce DSi concentrations. We argue that the weathering of andosols constitutes the most important source of DSi to the lakes and fjords of northern Chilean Patagonia, explaining the particularly high regional rates of biogenic silica production. Copyright © 2015 John Wiley & Sons, Ltd.

KEYWORDS: andosols; volcanic glass; dissolved silica; northern Chilean Patagonia; aquatic productivity

Introduction

Dissolved silica (DSi) is considered as one of the main nutrients in marine and lacustrine environments. It is especially important for the growth of diatoms, which are responsible for approximately 30% of global ocean productivity, and up to 70% of productivity in nearshore and estuarine areas (Nelson *et al.*, 1995). The biogeochemical role of DSi is particularly important in fjords, which were recently recognized as oceanic hotspots for organic carbon burial (Smith *et al.*, 2015). Compared to the rest of southern South America, the fjords of northern Patagonia (44–48°S) present the highest input of DSi and the highest rates of diatom productivity (Aracena *et al.*, 2011; Torres *et al.*, 2014). As a result, the carbon buried in the regional fjords is predominantly of aquatic origin (Sepúlveda *et al.*, 2011). In addition to promoting high fjord productivity, DSi inputs also limit diatom productivity along the Pacific coast (Torres *et al.*, 2014).

It is generally believed that the DSi riverine input to lake and coastal environments is controlled by a combination of factors including regional geology, climate, topography, and meltwater input (Torres *et al.*, 2014). For northern Chilean Patagonia, it has been proposed that volcanic activity could be responsible for the high DSi concentrations observed in the continental and coastal surface waters (Torres *et al.*, 2014). Although the influence of andosol distribution on the geochemistry of dissolved and suspended loads in north Patagonian rivers was mentioned in Bertrand *et al.* (2012), the degree of this influence remains largely unknown.

Due to the high volcanic activity in the Andes, andosols are very widespread in Chile. They are found between 36 and 47° latitude, where they cover most of the Andes and the Central Valley (Gut, 2008). Andosols have mostly been studied in south-central Chile (36–41°S), where authors have demonstrated that these soils were formed on volcanic ash that continuously accumulated after the glacial retreat (Laugenie, 1982;

McCurdy, 2003; Bertrand and Fagel, 2008). While similar soils are known to occur as far south as 47° (Gut, 2008), their exact distribution, lateral variations in thickness, composition, and/or parent material remain largely unknown. Current information on soils in this region is limited to rough maps of volcanic ash soil extension (Gut, 2008) and localized studies of very specific soil properties (Grez, 1984; Pfeiffer *et al.*, 2010). Moreover, major differences exist between northern Patagonia (44–48°S) and south-central Chile, such as: (a) the age of deglaciation (which occurred earlier in south-central Chile; Hulton *et al.*, 2002; Turner *et al.*, 2005; Glasser *et al.*, 2012), and therefore the duration of accumulation of volcanic ash; (b) climate, which is much more humid year-round in Patagonia (Garreaud *et al.*, 2009); and (c) location of the volcanoes compared with the drainage basins (mostly to the east in south-central Chile and to the west in northern Chilean Patagonia (Fontijn *et al.*, 2014). Accordingly, the conclusions obtained on the volcanic ash soils of south-central Chile cannot simply be extended to Chilean Patagonia.

This paper focuses on investigating the influence of andosols on riverine silica input to the fjords of northern Chilean Patagonia. First, andosol thickness measurements are used to map the extent and spatial variability in thickness of the regional volcanic ash soils. Selected profiles are then examined to assess the impact of weathering on the mineralogical and geochemical properties of andosols, and hence estimate the importance of silica leaching. Finally, the contribution of andosol weathering to the dissolved silica loads in regional rivers is examined for five distinct watersheds.

Setting

The landscape of northern Chilean Patagonia (44–48°S) is characterized by a complex network of islands and channels. It contains many fjords and lakes that were formed by extensive glacial erosion from the Patagonian Ice Sheet (PIS) during the Quaternary. Glacial retreat after the LGM resulted in the separation of the PIS into the northern Patagonian Icefield (NPI; Figure 1) and the southern Patagonian Icefield (SPI), and it uncovered most of the study region. Most of the NPI outlet glaciers flow into fjords towards the west and into proglacial lakes and rivers towards the east.

The regional geology consists mainly in granitoids, i.e. the North Patagonian Batholith, and volcanic rocks that were deposited during the Mesozoic and Cenozoic times (Figure 1; Pankhurst *et al.*, 1999). Metamorphic basement complexes and associated magmatic rocks (eastern Andean metamorphic complex and Chonos metamorphic complex; Figure 1) occur in the western and southern part of the study region. Mid-Cenozoic volcanic and sedimentary deposits, represented by the Traiguén Formation (Figure 1), occur along the Liquiñe-Ofqui Fault System (LOFS; Hervé *et al.*, 1995), which is a large NNE–WWS trending tectonic feature (Figure 1). The LOFS also controls the location of most large stratovolcanoes and of many of the small monogenetic Holocene eruptive centers (López-Escobar *et al.*, 1995).

Five volcanoes (Melimoyu, Mentolat, Cay, Maca, and Hudson) are located in the studied region. They all belong to the southern part of the southern volcanic zone of the Andes which consists in a continuous arc of stratovolcano complexes and volcanic fields with compositions ranging from tholeiitic, high-Al basalts to basaltic andesites, although andesites, dacites, and rhyolites can also occur (López-Escobar *et al.*, 1977, 1993, 1995; Hickey-Vargas *et al.*, 1984, 1989; Hickey *et al.*, 1986; Futa and Stern, 1988; Gerlach *et al.*, 1988). Of these five volcanoes, Hudson is by far the most active. It was the source of four large explosive postglacial eruptions that were dated at 17 400, 6700, and 3600 cal yr BP, and 1991 AD (Naranjo and Stern, 1998; Weller *et al.*, 2014), and of many smaller eruptions that are represented by thin tephra layers in regional sediment cores (Naranjo and Stern, 1998; Bartels, 2012; Weller *et al.*, 2014). The most recent volcanic activity of the Hudson was recorded in 2011 AD (Weller *et al.*, 2014). No historical activity has been reported for Mentolat, Melimoyu, Cay, and Maca volcanoes, although tephra layers associated with Holocene explosive eruptions of Melimoyu, Mentolat and Maca were described in lake sediments and proximal terrestrial outcrops (Naranjo and Stern, 2004; Stern *et al.*, 2015).

Precipitation patterns in southern South America display a strong zonal asymmetry due to the orographic high of the Andes and the dominating humid southern Westerlies coming from the Pacific Ocean (Figure 2). The western side of the Andes is dominated by a hyperhumid climate (Garreaud *et al.*, 2013) with precipitation reaching up to 7500 mm/yr (Miller, 1976). In contrast, on the leeside of the Andes, the forced subsidence causes precipitation to decrease rapidly to less than 250 mm/yr (arid climate; Figure 2). The west–east temperature gradient is not as pronounced as for precipitation. Temperature varies between 4 °C in austral winter (July) and 13 °C is austral summer (January), with an annual average around 8 °C (Domic Kuscevic *et al.*, 2000; Sagredo and Lowell, 2012).

Present-day vegetation distribution mainly reflects the west–east precipitation gradient (Figure 2). Along the Pacific Ocean vegetation consists in evergreen north Patagonian rainforests, and it evolves towards a Mediterranean grass steppe close to the Chile–Argentina border (Luebert and Pliscoff, 2006). In between the western rainforests, conifer evergreen forests occur at the coast and interior. At higher altitudes, vegetation is dominated by deciduous forest (Figure 2). Moorlands cover the Taitao Peninsula and the hyperhumid fjord and island area south of 47°S. The Eastern Patagonian arid landscape is dominated by shrubland and gramineous steppe (Figure 2).

Several large rivers draining northern Chilean Patagonia, i.e. Cisnes, Aysen, Baker, Gualas, and Exploradores, discharge large amounts of fresh water into the fjords and the adjacent eastern Pacific Ocean (Figure 1). Both Cisnes and Aysen are nival rivers with higher discharge in spring (Calvete and Sobarzo, 2011), whereas Gualas, Exploradores, and Baker rivers display a glacial regime due to their proximity to the NPI (Dussaillant *et al.*, 2012). The latter is also the largest river of Chile (highest mean discharge).

Materials and Methods

Sampling

The samples and data used in this study were collected during two field expeditions in January–February 2012 and 2013. Volcanic ash soil thickness was measured in quarries, along road cuts, or along river cuts where anthropogenic influence was minimal. The profiles selected for investigation have a relatively flat top, flat contact with the underlying deposits, and parallel internal structures, when visible. Sixty-eight profiles were described (lithology, structures, and Munsell color), photographed, and the thickness of the volcanic ash deposits was measured by placing a tape meter vertically against the section. Profiles were labeled APXX-YY, with AP standing for 'Andosol Profile', XX referring to the year of measurement, and YY representing the profile number (Figure 3). Their location was recorded with a Garmin Etrex GPS (Supplementary information, Table S1). Sites that were visited but did not contain andosols were also recorded (Figure 3 and Figure S2 in Supplementary information). Three of the andosol profiles (AP12-04, AP12-02 and AP13-11; Figures 1–3) were sampled for geochemical and mineralogical analysis every five (AP12-02 and AP13-11) or ten (AP12-04) cm, depending on the thickness of the profile.

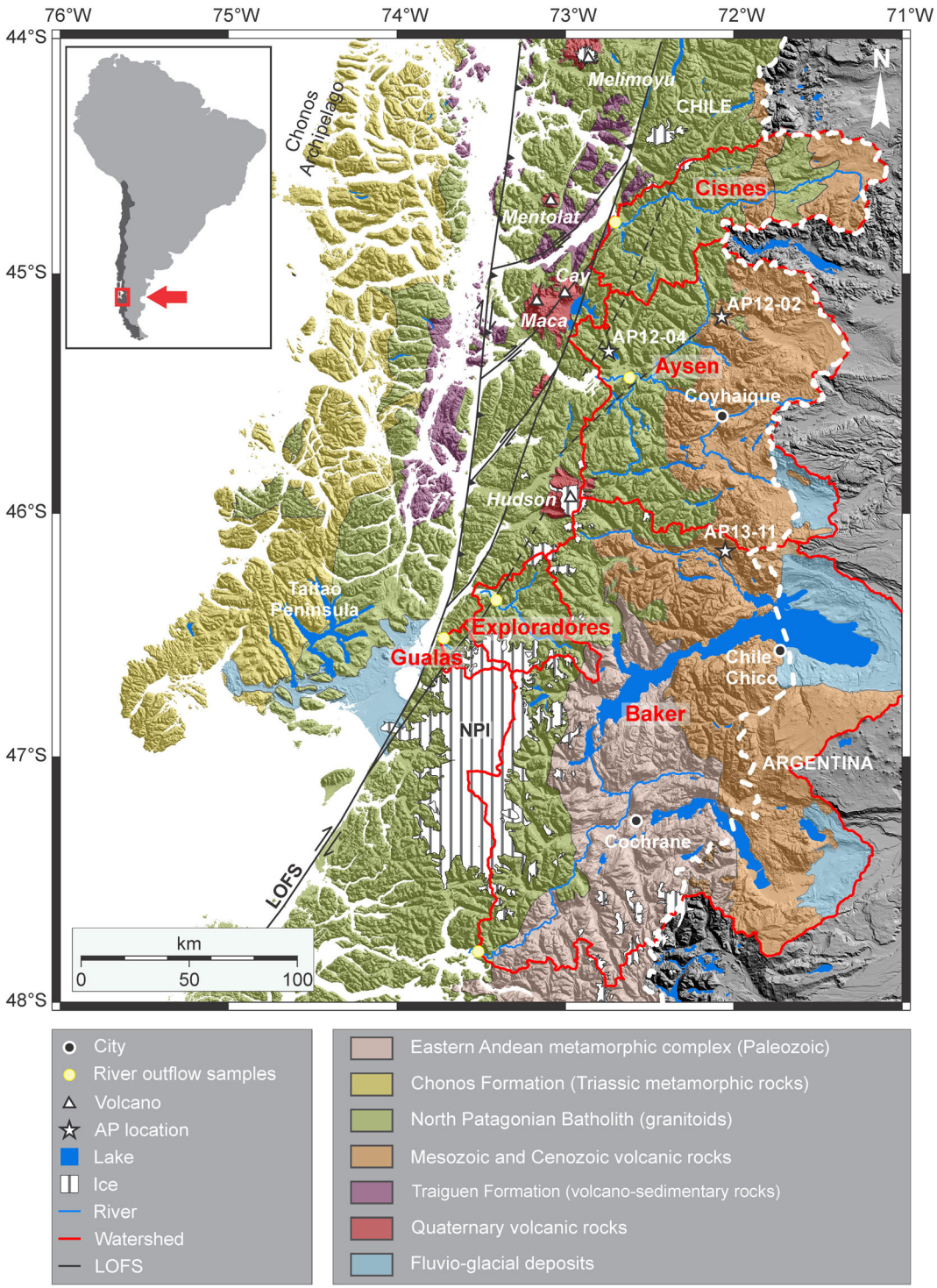

Figure 1. Geological map of the study region, displaying the location of the five studied watersheds (from north to south: Cisnes, Aysen, Exploradores, Gualas, and Baker), and the main river systems draining these basins. NPI and LOFS stand for Northern Patagonian Icefield and Liquiñe-Ofqui Fault System (Cembrano and Lara, 2009), respectively. The dashed white line represents the Chile-Argentina border. The lithological units are based on the geological maps of Chile (Sernageomin, 2003) and Argentina (Segemar, 1998). This figure is available in colour online at wileyonlinelibrary.com/journal/espl

In addition to the soil samples, this study makes use of river water samples that were collected in October–November 2011 at the outflow of the main rivers draining northern Chilean Patagonia and flowing to the fjords (Figure 1). For each river, four to five samples were collected along a vertical profile, and preserved in I-Chem cubitainers. They were filtered within 24 h of sampling using a pressurized filtration system equipped with a 90 mm diameter PEF membrane (pore size 0.22 µm). These filtered samples were preserved in pre-acidified 125 ml HDPE Nalgene bottles and kept at 4 °C until analysis. Additional river water samples were collected monthly at the outflow of Aysen and Baker rivers in 2008–2010. These samples were collected with a syringe and filtered on the field using 0.45 µm nitrocellulose filters. They were stored in high density plastic vials at room temperature until analysis.

Andosol isopach mapping

An isopach map of volcanic ash soil thickness was created using Surfer 9, based on the values measured at the 68

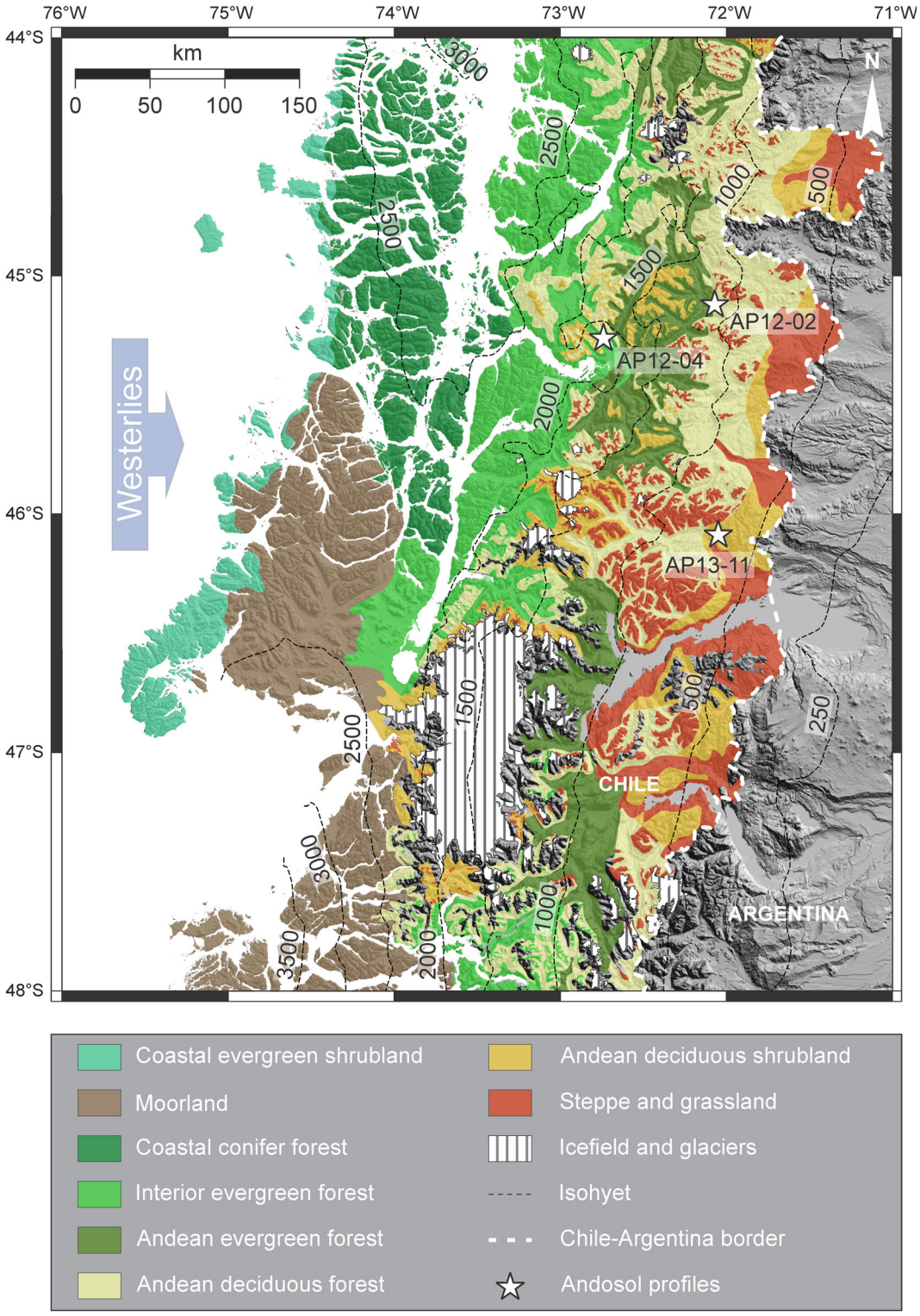

Figure 2. Vegetation map (modified after Luebert and Pliscoff, 2006) and annual precipitation (from Hijmans *et al.*, 2005) of northern Chilean Patagonia. The distribution of the vegetation units is clearly related to the strong west–east precipitation gradient. The white stars represent soil profiles AP12-04, AP12-02, and AP13-11, which receive precipitation amounts of approximately 2600, 1400, and 725 mm/yr, respectively. This figure is available in colour online at wileyonlinelibrary.com/journal/espl

andosol profiles. Gridding was made with the *Kriging* method. In addition to the AP thickness data, additional points were added to the database to provide additional constraints in areas were field data are scarce. These extra locations include thickness values assigned to volcanoes based on their postglacial eruptive history, points reflecting areas where volcanic ash soils are absent, and western extent of the occurrence of andosols, as indicated on the soil map of southern South America (Gut, 2008). Ash fall distribution maps of the largest eruptions of Hudson (Naranjo and Stern, 1998), Maca, and Mentolat volcanoes (Naranjo and Stern, 2004) were used to enhance the final shape of the volcanic ash soil thickness map in the immediate vicinity of the volcanoes (<20 km). Since gridded thickness values <0.1 m do not correspond to andosols on the field (volcanic ash was likely not preserved), 0.1 m was considered as the limit of andosol cover. Consequently, this map was used to calculate the volume and average thickness of the volcanic ash deposited in each watershed, using the volume calculation tool in Global Mapper 16.

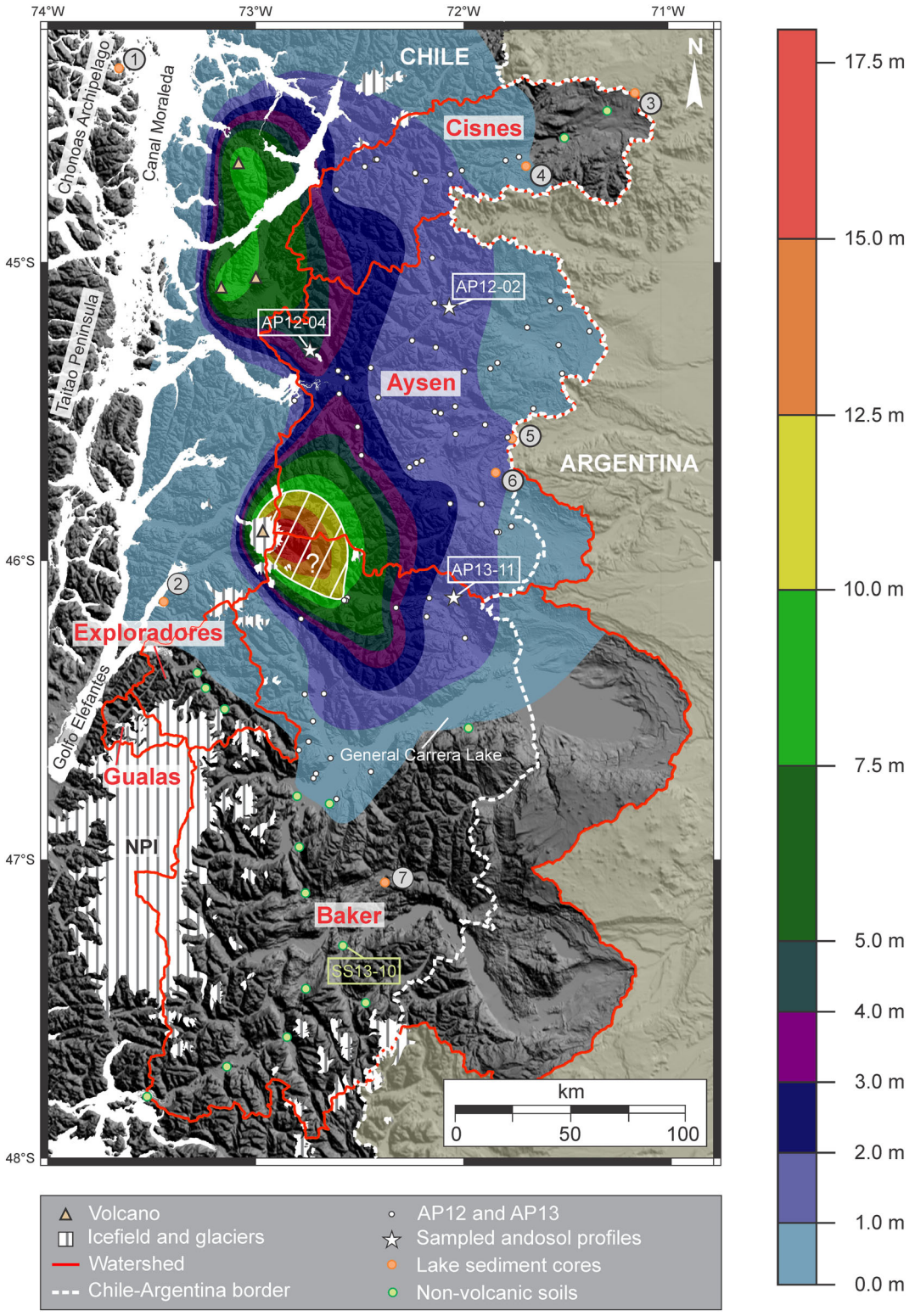

Figure 3. Volcanic ash soil thickness map of northern Chilean Patagonia with indication of the investigated profiles AP12-04, AP12-02, and AP13-11. The green dots represent locations where soils developed on non-volcanic material were described during the 2013 field expedition (e.g. histosol SS13-10 in Figure S2). The isopach map was validated using lake sediment cores (orange dots) with known cumulated post-glacial tephra thickness: (1) Laguna Oprasa (3 cm; Haberle and Lumley, 1998); (2) Laguna Miranda (10 cm; Haberle and Lumley, 1998); (3) Lago Shaman (9 cm; de Porras *et al.*, 2012); (4) Mallín El Embudo (36 cm; de Porras *et al.*, 2014); (5) Lago Castor (79.9 cm; Van Daele *et al.*, 2016); (6) Mallín Pollux (>42 cm; Markgraf *et al.*, 2007); and (7) Lago Augusta (12 cm; Villa-Martínez *et al.*, 2012). The striped area near Hudson volcano highlights a region where volcanic ash soil thickness may have been overestimated. This figure is available in colour online at wileyonlinelibrary.com/journal/espl

Soil sample pre-treatment

The three sub-sampled profiles (AP12-04, AP12-02 and AP13-11; Figures 4–6) come from sites with precipitation amounts typical for the region, ranging from 725 mm/yr (AP13-11) to 2600 mm/yr (AP12-04) (Figure 2). Profile AP12-02 is located in an intermediate setting, with precipitation values averaging around 1400 mm/yr. Before analysis, the soil subsamples were oven-dried at 60 °C and manually sieved at 90 µm, using a 10 cm Ø Retsch stainless steel test sieve. Analyses were conducted on only the finest fraction (<90 µm), ensuring a limited influence of grain-size on the analytical results. This is

particularly important for andosols since volcanic deposits can contain very coarse (>10 cm Ø) particles, depending on the explosivity of the successive eruptions.

Mineralogy

The mineralogical composition of every other sample was determined by X-ray diffraction (XRD) analysis. Before analysis, samples were prepared using the non-destructive Backside method (Brown and Brindley, 1980). Samples were analyzed on a Bruker D8-Advance diffractometer, which uses CuKα-radiations, and submitted to XRD between 5° and 45° 2θ. The step size was 0.02° and scan speed was set at 2 s/step. The resulting diffractograms were semi-quantified (wt.%) following Cook *et al*. (1975) where the intensity of the principal diffraction peak of each mineral was corrected by a multiplication factor (pyroxene: 5; K-feldspar: 4.3; amphibole: 2.5; plagioclase: 2.8; and quartz: 1). To determine the amorphous material content, the maximum height of the amorphous diffraction band was measured and multiplied by 75 following Bertrand and Fagel (2008).

Inorganic geochemistry

Elemental analysis of the soil samples was performed by X-ray fluorescence (XRF) on fused Li-borate glass beads after loss on ignition at 1000 °C. Analyses were performed using an ARL PERFORM-X 4200. Duplicate analyses of 105 reference materials indicate an accuracy (1σ) of 0.506% and 0.232% for SiO_2 and Al_2O_3, respectively.

DSi concentrations of the October–November 2011 river water samples were measured using a Varian 720-ES ICP-OES. For the river water samples collected in 2008–2010, DSi was determined spectrophotometrically using a modified version of the method of Strickland and Parsons (1968), according to the protocols of Joint Global Ocean Flux Study (JGOFS, 1996). Samples were reacted with ammonium molybdate and metol-sulfide was used as a reducer.

Results

Volcanic ash soil thickness map

The isopach map of volcanic ash soils in northern Chilean Patagonia (Figure 3) displays thickness values decreasing logarithmically with increasing distance from the source volcanoes Hudson, Cay, Maca, and Mentolat. The decrease is very steep towards the west and more gentle towards the east. To the west, the volcanic ash soil cover extends to the north–south oriented Elefantes-Moraleda fjords. The southern extent of the volcanic ash soils runs through the Baker and Exploradores watersheds, where it coincides with a large part of General Carrera Lake. The eastern boundary of the volcanic ash soils has only been mapped in the Cisnes drainage basin. Towards the east, the andosol cover extends into Argentina.

The area with the thickest volcanic ash soils is located to the east and southeast of Hudson volcano, reflecting the large explosive eruptions of this volcano during the Holocene (Naranjo and Stern, 1998). Only one watershed (Aysen) is completely covered by andosols (Figure 3; Table I). Its average volcanic ash soil thickness reaches 2.34 m (Table I). In contrast, volcanic ash soils are absent from the small Gualas catchment. The volcanic ash soil volume is higher in Aysen watershed (28.82 km^3) than in the four other watersheds combined (Table I). This is directly related to its location immediately to the east of most of the regional active volcanoes (Figure 3).

Bulk mineralogy

The three profiles that were investigated for mineralogy and geochemistry have a thickness ranging from 134 to 450 cm (Figures 4–6). They consist of light brown or light yellow orange to black layered deposits of coarse silt and sand with distinct pumice layers or pumice particles that are imbedded in the deposits. The profiles are underlain by granitic bedrock (AP12-04; Figure 4) or pre-Holocene fluvio-glacial sediments (AP13-11 and AP12-02; Figures 5 and 6).

All the samples analyzed by XRD contain amorphous material, quartz, plagioclase, K-feldspar, and pyroxene (Figures 4–6). Amphibole was detected in only two samples (AP12-02-20 and AP13-11-0).

Profile AP12-04 (Figure 4) is dominated by amorphous particles (46 ± 11%; 1σ), and plagioclase (33 ± 11%), without any clear trend with depth. This profile contains the lowest quartz amount (1 ± 1%). The mineralogy of profile AP12-02 (Figure 5) is similarly dominated by amorphous particles (47 ± 9%) and plagioclase (26 ± 6%), which are both slightly decreasing towards the bottom of the profile due to the increasing quartz content (9 ± 9%). In AP12-02, amphibole occurs in one of the fluvio-glacial samples (AP12-02--20; 10%). Although profile AP13-11 (Figure 6) is also dominated by amorphous particles (48 ± 12%) and plagioclase (24 ± 8%), these two components clearly decrease towards the bottom of the profile, to the advantage of quartz, which reaches concentrations above 20%. The only exception to these well-marked trends is for sample AP13-11-100, which shows relatively high quartz concentrations. One can also notice that the highest values of amorphous material are consistent with the presence of coarse pumice layers in samples AP13-11-90, AP13-11-80, and AP13-11-70. In profiles AP13-11 and AP12-02 (Figures 5 and 6), i.e. the two profiles underlain by fluvio-glacial deposits, the highest quartz contents occur in the fluvio-glacial deposits and at the base of the andosol profiles, indicating the incorporation of quartz particles in the lowermost volcanic ash deposits. This is in contrast with profile AP12-04 (Figure 4), which covers granitic bedrock, and does not contain significant amounts of quartz.

Table I. Calculated volcanic ash volumes deposited in the five studied watersheds compared to average annual precipitation (Hijmans *et al*., 2005), granite coverage (Segemar, 1998; Sernageomin, 2003), glacier coverage (Glasser *et al*., 2011), average slope, and lake coverage

Drainage basin	Surface area (km^2)	Surface area covered by andosols (%)	Volume volcanic ash (km^3)	Average andosol thickness (m)	Average precipitation (mm/yr)	Granite coverage (%)	Glacier coverage (%)	Average slope (degrees)	Lake coverage (%)
Cisnes	5357	69.7	6.35	1.19	1181	69.2	1.4	18.0	0.6
Aysen	12 315	100.0	28.82	2.34	1101	41.7	0.1	16.8	1
Exploradores	1860	36.1	0.18	0.10	1553	95.6	17.3	23.6	0.0
Gualas	361	0.0	0.00	0.00	1742	100.0	54.1	23.2	0.0
Baker	29 396	26.7	18.88	0.64	707	20.6	8.0	15.1	8.1

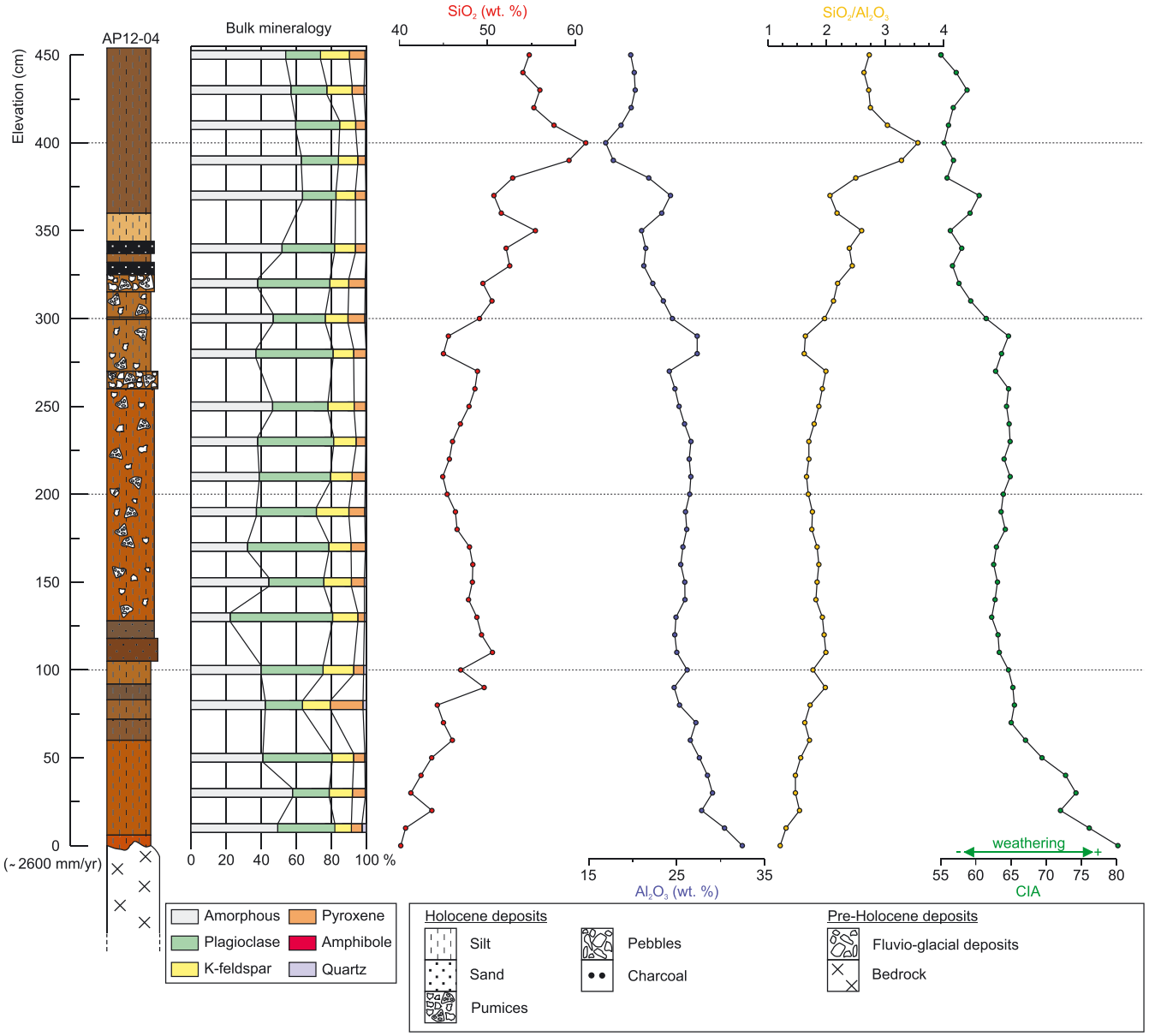

Figure 4. Lithology, mineralogy and geochemistry of profile AP12-04 (see Figures 1–3 for location). The CIA values were calculated after quartz correction (see section 'Nature of andosol parent material and weathering'). This figure is available in colour online at wileyonlinelibrary.com/journal/espl

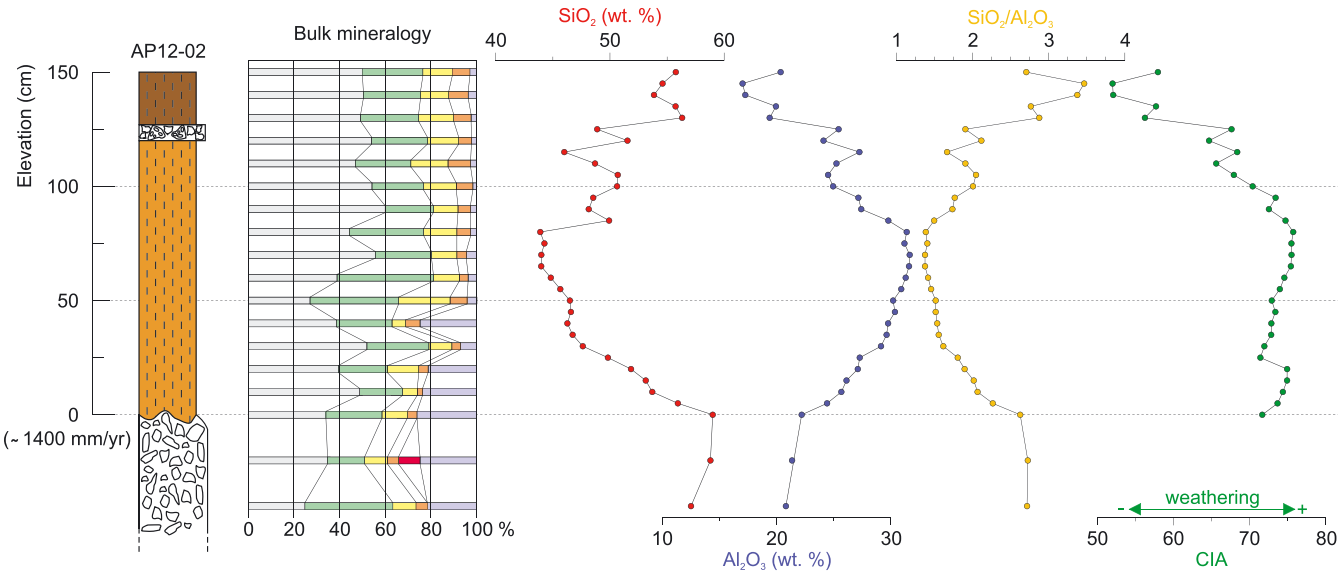

Figure 5. Lithology, mineralogy and geochemistry of profile AP12-02 (see Figures 1–3 for location). The CIA values were calculated after quartz correction (see section 'Nature of andosol parent material and weathering'). The legend is presented in Figure 4. This figure is available in colour online at wileyonlinelibrary.com/journal/espl

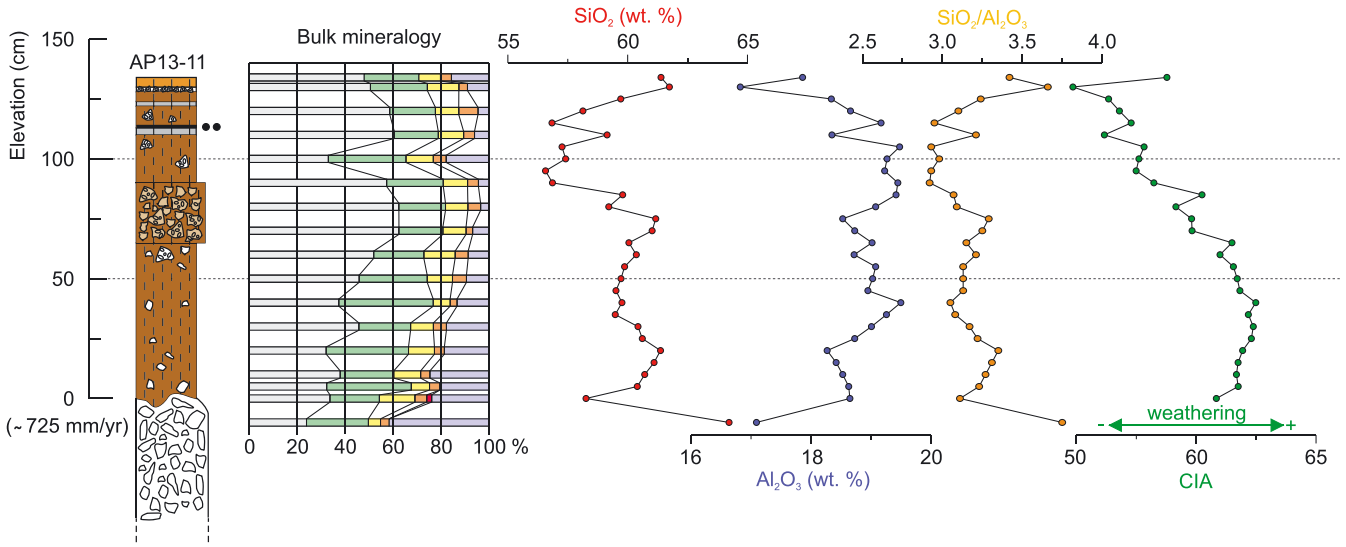

Figure 6. Lithology, mineralogy and geochemistry of profile AP13-11 (see Figures 1–3 for location). The CIA values were calculated after quartz correction (see section 'Nature of andosol parent material and weathering'). The legend is presented in Figure 4. This figure is available in colour online at wileyonlinelibrary.com/journal/espl

Geochemistry

Of the three investigated profiles, AP13-11 displays the highest average silica concentrations (59.67 ± 1.50 wt.%; 1σ; Figure 6), whereas in profiles AP12-04 (Figure 4) and AP12-02 (Figure 5) SiO_2 occurs in lower concentrations (49.04 ± 4.77 wt.% and 50.07 ± 4.88 wt.%, respectively). Al_2O_3 concentrations show large differences between profiles. The lowest values are recorded in AP13-11 (18.83 ± 0.57 wt.%), followed by profile AP12-04 (24.85 ± 3.29 wt.%) and profile AP12-02 which contains on average 26.61 ± 4.30 wt.% Al_2O_3. The three profiles show a decrease in SiO_2 and an increase in Al_2O_3 with depth. The SiO_2/Al_2O_3 ratio decreases with depth in profile AP12-04 (Figure 4) but does not show any continuous and consistent trend in AP12-02 and AP13-11 (Figures 5 and 6). The largest variability in elemental concentrations occurs in the upper part of the profiles.

For each river, water samples collected along vertical profiles at the river outflows have similar DSi concentrations (Table II). Large differences in average DSi concentrations however occur from river to river (Table II) with concentrations ranging from 0.56 mg L^{-1} (Gualas) to 3.66 mg L^{-1} (Aysen). The resulting DSi flux estimates vary from 1.48 × 10^9 g/yr to 66.37 × 10^9 g/yr (Table II). DSi concentrations measured monthly throughout the year (2008–2010) seem to display seasonal variations (Supplementary information, Figures S3 and S4).

Discussion

Validation of the isopach map

Before using the soil thickness map, we compared the results shown in Figure 3 with the cumulated thickness of postglacial tephras preserved in lake sediment cores. A total of seven lake sediment cores were examined (Figure 3). Tephra preserved in Laguna Oprasa (3 cm) and Laguna Miranda (10 cm) (Haberle and Lumley, 1998), which are located on the western side of our study area, confirm the western extension and thickness of the volcanic ash soils. Tephra preserved in sediment cores from Lago Shaman and Mallín El Embudo, both located in the upper part of Cisnes watershed, show cumulative thickness of 9 cm (de Porras *et al.*, 2012), and 36 cm (de Porras *et al.*, 2014), respectively, which is in agreement with the location of the 10 cm isopach in-between these two lakes (Figure 3).

Further south in Lago Castor (Van Daele *et al.*, 2016) and Mallín Pollux (Markgraf *et al.*, 2007), cumulated tephra thicknesses reach 79.9 cm and > 42 cm (not all tephras were described in details), respectively. These two records seem to contain slightly less tephra than that represented in Figure 3, although volcanic ash soil thickness in profile AP12-01, which is located on the shore of Lago Castor, clearly reaches 120 cm (Supplementary information, Table S1). This discrepancy may be due either to the non-representativeness of site AP12-01, which is located in a valley where tephra can locally over-accumulate, and/or to the non- or incomplete deposition of low density (pumice-rich) tephra in lakes Castor and Pollux.

Finally, the sediment record of Lago Augusta, which is located in the northernmost part of Baker watershed, contains a cumulated tephra thickness of 12 cm (Villa-Martínez *et al.*, 2012), which is slightly higher than values mapped in that region (<10 cm). This can be explained by the lake environment yielding better preservation potential of tephra deposits than terrestrial environments, especially thin deposits (Fontijn *et al.*, 2014).

In general the isopach map is in excellent agreement with cumulated thickness of tephra layers in lakes. Although minor differences exist, they can generally be explained by the reworking of tephra in terrestrial environments and their inhomogeneous deposition in lakes (Bertrand *et al.*, 2014).

Table II. DSi flux estimates based on river discharge and DSi concentrations measured in spring (October–November) 2011

Watershed	DSi concentrations (mg/L) ± 1σ	River discharge (m^3/s) ± 1σ	DSi flux (×10^9 g/yr)
Cisnes	1.91 ± 0.05	273 ± 5	16.44
Aysen	3.66 ± 0.08	575 ± 12	66.37
Exploradores	0.96 ± 0.06	399 ± 5	12.08
Gualas	0.56 ± 0.02	84 ± 9	1.48
Baker	1.37 ± 0.09	1120 ± 22	48.39

Spatial variability in andosol thickness

The volcanic ash soil thickness map (Figure 3) clearly demonstrates the significant control of the Westerlies on the distribution of andosols in northern Chilean Patagonia. The volcanic ash

soils are thick and widespread on the eastern side of the volcanoes whereas their thickness sharply decreases to the western side. The decline in thickness towards the west is so steep that andosols are replaced by cambisols and histosols within less than 50 km to the west of the volcanoes (e.g. Taitao Peninsula and Chonos Archipelago, Figure 3). Comparison of the volcanic ash soil extent (Figure 3) with the soil map of Gut (2008) indicates differences for the southern limit of andosols. Gut's map illustrates the presence of andosols to the south of General Carrera Lake, up to latitudes >47°S, whereas no volcanic ash soils were observed on the field in this area. Our detailed soil thickness map demonstrates that the southern limit of the volcanic ash soils is restricted to approximately 46.5°S, with a central lobe reaching almost 47°S (Figure 3).

The observation that the andosols are thick and extend far to the east of the regional volcanoes is in direct agreement with the distribution of tephras emitted by the regional volcanoes during the Holocene (Naranjo and Stern, 1998, 2004; Fontijn *et al.*, 2014). More specifically, the volcanic ash distribution map (Figure 3) clearly displays two distinctive lobes on the eastern side of Hudson volcano. The shape of these lobes is similar to the isopachs of the three largest Holocene eruptions of the Hudson volcano. The first lobe, located in the southern region, mimics the 6700 BP and 1991 AD eruption events, for which the thickness of volcanic ash is declining in a southeastward direction (S40°E; Naranjo and Stern, 1998), whereas the second lobe, situated directly to the east of the volcano, roughly follows the lobe of the 3600 BP eruption, where the axis of dispersal is in a more easterly direction. Moreover, the lobe visible on the eastern side of the volcanoes Cay and Maca (Figure 3) matches the distribution of volcanic ashes of the 1540 BP Maca eruption (Naranjo and Stern, 2004).

In addition to volcanic ash transport by the westerlies, another factor that may influence the gradual decrease in volcanic ash soil thickness towards the east is vegetation density. As mentioned in the section 'Sampling', the eastern part of the study region is characterized by a dry and sparsely vegetated steppe-dominated landscape that is very susceptible to wind erosion (Peri and Bloomberg, 2002; Villa-Martínez and Moreno, 2007). In such landscapes tephra preservation is restricted to sites where vegetation occurs, as demonstrated by Wilson *et al.* (2011) for deposits from the 1991 AD Hudson eruption.

Processes affecting andosol thickness at the local scale

Although the andosol thickness map presented above is accurate at the scale of northern Patagonia, several factors may affect the thickness of the volcanic ash soils at the local scale.

First, volcanic ash fall deposits are not entirely independent of pre-existing topography. This influence is particularly important on steep slopes and above the treeline, where tephra is prone to erosion and remobilization.

Second, tephra thickness may have been overestimated in the nearby vicinity of the volcanoes since volcanic deposits near craters are generally too coarse and/or consolidated to allow formation of andosols (see striped area in Figure 3). Although the ash soil thickness map present values above 10 m on the flank of regional volcanoes, the highest volcanic ash soil thickness that was actually measured is 8.10 m (southeast of Hudson volcano; Figure 3). As a result, the calculated volume of volcanic ash soils may be slightly overestimated.

A third factor is the age of deglaciation, which was not synchronous over Patagonia (Hulton *et al.*, 2002). Regions that deglaciated early have accumulated volcanic ash during a longer period of time.

Nature of andosol parent material and weathering

The mineralogical composition of the investigated samples, which is dominated by amorphous material, plagioclase, K-feldspar, and pyroxene (Figures 4–6), confirms the volcanic nature of the parent material. The high amount of plagioclase (24 ± 8%, 26 ± 6%, and 33 ± 11% for profiles AP13-11, AP12-02, and AP12-04, respectively) and pyroxene (5 ± 1%, 6 ± 2%, and 7 ± 2% for profiles AP13-11, AP12-02, and AP12-04, respectively) in the volcanic ash soil samples is consistent with their origin from the regional SVZ volcanoes since these minerals are commonly found in basalts and andesitic basalts (Shoji *et al.*, 1993). The high amounts of material quantified as amorphous by XRD is the result of the combined contribution of volcanic glass, organic matter, and non-crystallized clays. These values are comparable with the amorphous content found in andosol outcrops from south-central Chile (Bertrand and Fagel, 2008). Darker horizons generally correspond to levels enriched in organic matter (Figures 4–6). Proper A horizons are, however, absent since volcanic ash accumulated in several phases during the Holocene, rapidly burying the immature organic horizons.

The only minerals that were observed in the volcanic ash soil samples and that are not related to regional eruptive volcanism are quartz and amphibole (Figures 4–6; D'Orazio *et al.*, 2003; Stern *et al.*, 2007; Ruggieri *et al.*, 2011). The presence of these two minerals in profiles AP13-11 and AP12-02 can easily be explained by the fluvio-glacial nature of the underlying deposits, which are generally composed of eroded granitoids (Nelson *et al.*, 1988; Pankhurst *et al.*, 1999; Bertrand *et al.*, 2012) and therefore likely provided the quartz and amphibole grains that occur at the bottom of the profiles. This interpretation is in agreement with results previously obtained on andosol profiles underlain by fluvio-glacial deposits in south-central Chile (Bertrand and Fagel, 2008), where the lower parts of the andosol profiles were similarly enriched in quartz and amphibole. Incorporation of quartz and amphibole is negligible in profile AP12-04 since it is underlain by granitic bedrock. The very low amount of quartz in profile AP12-04 could also be related to higher dilution by volcanic ash since this profile is three times thicker than profiles AP13-11 and AP12-02 due to its location close to the source volcanoes (Figure 1). The particularly high quartz content of profile AP13-11 throughout is probably due to its particular location downwind of mountain ranges (e.g. Cerro Castillo) that have likely been affected by pro-glacial erosion processes during most of the Holocene, hence providing a continuous source of fine-grained quartz particles to site AP13-11. Similarly, anthropogenic contamination from road construction, which typically uses local fluvio-glacial deposits, can explain the higher quartz content in the uppermost two samples (Figure 6).

The presence of quartz (of non-volcanic origin) at the bottom of andosol profiles AP12-02 and AP13-11 has a large influence on the geochemical composition of these two profiles, masking the effects of weathering on volcanic ash. To discuss the weathering of the volcanic ash fraction of the andosols only, the elemental compositions were recalculated on a quartz-free fraction, i.e. after subtraction of Si contained in quartz as measured by XRD. After correction, all three profiles display clear decreasing Si and increasing Al trends with depth (Figure 7 and Figure S1 in Supplementary information), indicating stronger weathering for older deposits. On the TAS plot (Figure 7), one can notice that the uppermost, i.e. less weathered, samples of the three profiles reflect a basaltic to andesitic composition, in agreement with volcanic material emitted by the regional volcanoes. The effect of weathering can be seen in Figure 7,

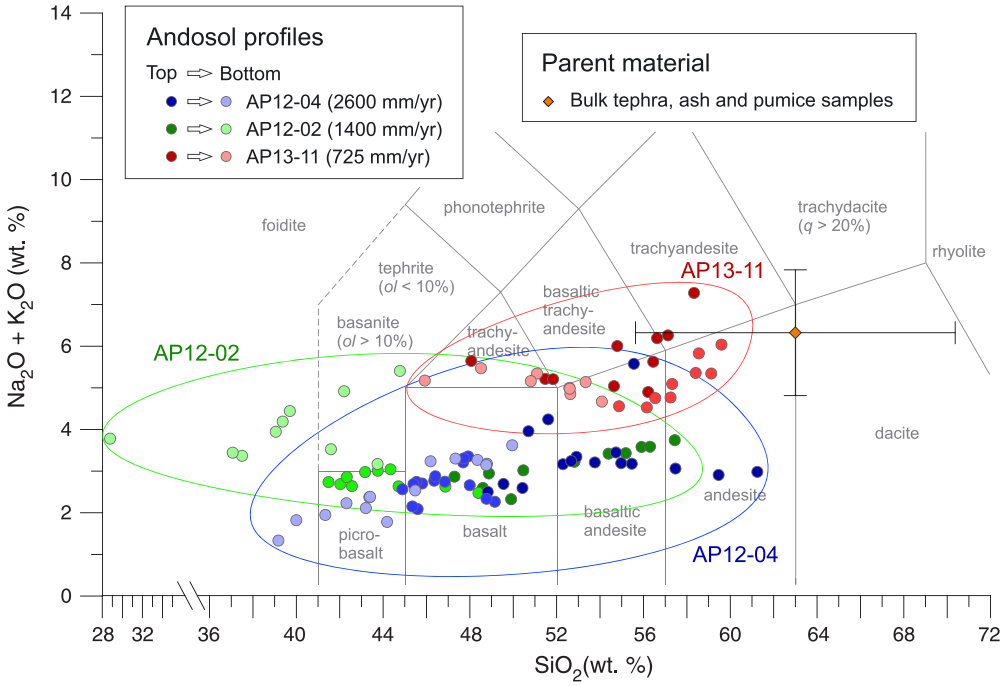

Figure 7. TAS plot of the samples collected in andosol profiles AP13-11, AP12-02, and AP12-04. SiO_2 and Na_2O+K_2O percentages were corrected for quartz as described in the section 'Nature of andosol parent material and weathering'. For comparison, the average of regional bulk tephra, ash, and pumice samples (SiO_2 = 62.98 ± 7.37 wt.%; Na_2O+K_2O = 6.32 ± 1.51 wt.%; n=19; Fuenzalida, 1974; Naranjo and Stern, 1998, 2004) is also shown. The volcanic ash soils are depleted in SiO_2, Na_2O, and K_2O compared with the parent material since these elements are leaching during weathering. This figure is available in colour online at wileyonlinelibrary.com/journal/espl

which displays a 23, 50, and 36% decrease in SiO_2 from top to bottom of profiles AP13-11, AP12-02, and AP12-04, respectively. This marked decrease in silica concentrations likely represents the weathering of the andosols parent material, which is dominated by the dissolution of volcanic glass, which is known to be prone to weathering (Shoji *et al.*, 1993). In addition to silica concentrations decreasing downwards, Figure 7 also displays moderate leaching of the alkali elements, with Na_2O+K_2O decreasing by 14 and 33% relatively for profiles AP13-11 and AP12-04, respectively, whereas a relative increase of 42% in Na_2O+K_2O is displayed for profile AP12-02. This increase may be due to the influence of the underlying fluvio-glacial deposits, which, in addition to quartz, also contain Na- and/or K-rich minerals (e.g. feldspar). The downward increase in weathering is also confirmed by the values of the Chemical Index of Alteration (CIA; Nesbitt and Young, 1982), which increase from 50–55 to 61–80 (Figures 4–6).

Although the volcanic ash soils of northern Chilean Patagonia are relatively recent, i.e. they only developed after the last glaciation, the base of the profiles is already highly weathered. Two factors can explain the regional high weathering rates. First, tephra emitted by the regional volcanoes has a basalt to andesitic basalt composition (Figure 7), and Si-poor tephras have higher weathering rates than more siliceous (rhyolitic) deposits (Shoji *et al.*, 1993; Wolff-Boenisch *et al.*, 2004). Second, the regional climate is hyperhumid year-round, enhancing weathering rates and therefore increasing the leaching of Si, in particular from fresh volcanic glass (Arnalds, 2012). The effect of precipitation on andosol weathering is particularly clear when comparing profiles AP13-11 and AP12-02 (Figure 7). Although the two profiles have approximately the same thickness, profile AP12-02 is more weathered (lower SiO_2 and alkali concentrations, and much higher CIA values at the base of the profile), due to its location in a high precipitation area (1400 mm/yr) compared with AP13-11 (725 mm/yr).

Influence on river chemistry

It was recently suggested that the postglacial volcanic ash soils may explain the particularly high supply of DSi to the fjords of northern Chilean Patagonia (Torres *et al.*, 2014). To assess the influence of andosols on DSi concentrations in north Patagonian rivers, we compared DSi concentrations measured in spring 2011 in the five main rivers that discharge into the fjords (Figure 1; Aysen, Cisnes, Baker, Exploradores, and Baker) with the average volcanic ash soil thickness of the corresponding watersheds (Table I). The results demonstrate a strong positive linear relationship (R^2=0.98, P<0.001; Figure 8(a)). Rivers that drain watersheds with thick volcanic ash soils, e.g. Aysen and Cisnes, systematically have higher DSi concentrations. Although the correlation presented in Figure 8 is based only on DSi values measured in spring 2011, seasonal variations in DSi concentrations are smaller than river-to-river differences (see whisker plots in Figure 8), making the correlation regionally robust and relatively independent of seasonal variations.

In addition to volcanic ash soil thickness, other factors or processes may influence DSi concentrations in Patagonian river systems.

First, the other soils occurring in the studied watersheds, i.e. cambisols and histosols, could possibly also contribute to the input of DSi in regional rivers. However, these soils are thin and highly immature (Figure S2) implying a very limited influence on DSi concentrations.

Another factor is the nature of the regional geological bedrock. As shown in Figure 1, the regional geology is dominated by granitoids (35%) and metamorphic rocks (18%). The correlation between the percentage of granitoids in each watershed (Table I) and DSi concentrations is however insignificant (R^2=0.31, P=0.33), suggesting that the nature of the geological bedrock does not play an important role in controlling DSi differences in north Patagonian rivers. A third factor is climate. The correlation between precipitation (Table I) and DSi concentrations is however insignificant (R^2=0.22, P=0.43), meaning that differences in precipitation across northern Chilean

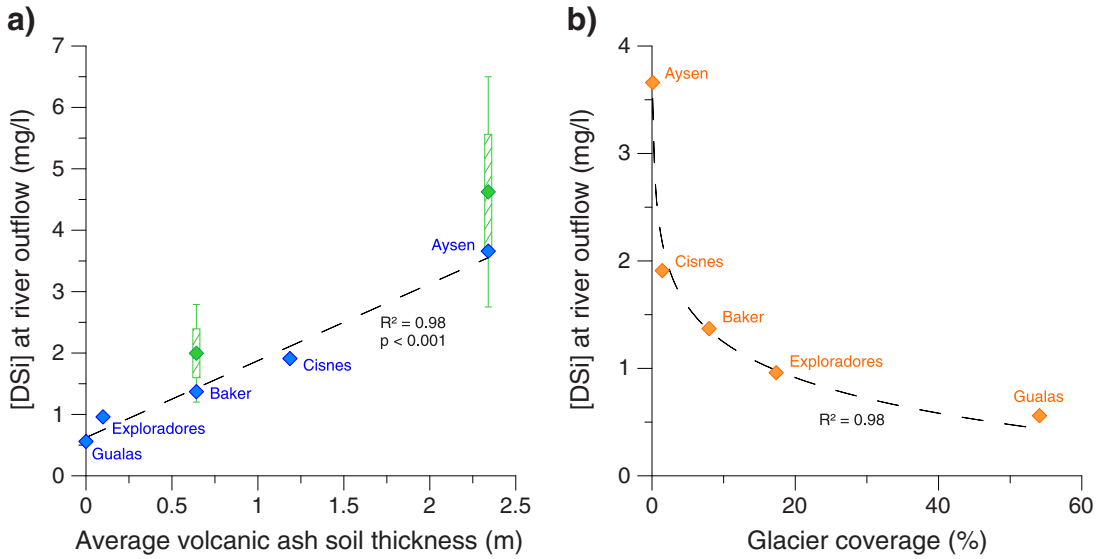

Figure 8. Relationships between DSi concentrations and (a) average volcanic ash soil thickness, and (b) glacier coverage (see Table I for data). DSi concentrations were measured on samples collected in austral spring at the outflow of Rio Cisnes, Rio Aysen, Rio Exploradores, Rio Gualas, and Rio Baker (see section 'Sampling'). Diamonds indicate DSi concentrations collected in austral spring 2011. The green box-whisker symbols indicate the range (1σ and 2σ) of seasonal DSi concentrations, from samples taken in 2008–2010. Average glacier coverage was calculated from Glasser *et al.* (2011). This figure is available in colour online at wileyonlinelibrary.com/journal/espl

Patagonian are not responsible for the regional differences in riverine DSi concentrations. Likewise, temperature is rather homogenous across the study region (Garreaud *et al.*, 2013) so it cannot be responsible for the observed variations in DSi. A direct consequence of this lack of relation between DSi concentrations and climate is that the influence of vegetation can also be excluded since the distribution of vegetation is mostly controlled by the longitudinal gradient in precipitation (Figure 2).

Another potentially important parameter is topography. The influence of topography on riverine DSi concentrations is based on the principle that on steep slopes, dissolution of andosols is lower because of the limited duration of the contact between water and soil particles (Andrews *et al.*, 2004). In Patagonia, this influence may be reinforced by the non-preservation of volcanic ash soils on the steepest slopes (Duffield *et al.*, 1979; Wright *et al.*, 1980; Cas and Wright, 1995). Correlation between average slope and DSi concentrations however indicates that this relation is negligible (R^2=0.38, P=0.27; Table I).

One variable that seems to significantly affect DSi concentrations is glacier coverage (R^2=0.98; Table I; Figure 8(b)). This significant relation can be explained by the high input of DSi-poor meltwater in regions where glacier coverage is high, such as the Gualas and Exploradores watersheds (Figure 1). The highly significant logarithmic correlation between these two variables may however be affected by the uneven distribution of glaciers, which predominantly occur in regions poorly covered with andosols (i.e. southern part of the study region, Figure 3).

Finally, since lakes have the ability to act as DSi traps (Conley *et al.*, 2000) lake coverage may also decrease riverine DSi concentrations. This influence is, however, minimal (R^2=0.00, P=0.96) in our study region, very likely because: (1) lake coverage is lower than 1% in most watersheds (Table I; Figure 1); and (2) most Patagonian lakes are ultra-oligotrophic, which limits DSi uptake (De Los Ríos-Escalante *et al.*, 2013).

Taken together, these results indicate that volcanic ash soil thickness is the primary variable controlling the large-scale differences in DSi concentrations in north Patagonian rivers. Although the influence of glacier coverage is also significant, it is not entirely independent of volcanic ash soil distribution, and the role of meltwater input is likely more important on shorter, i.e. seasonal, timescales (Supplementary information, Figure S3). The other major difference between the two variables is that the volcanic ash soils constitute the source of DSi while meltwater input dilutes the riverine DSi concentrations. Since glacier coverage is not linearly correlated with DSi (Figure 8), it is impossible to calculate the weight of each variable using a simple multiple regression analysis.

Our results have important implications for lake and fjord productivity. They imply that the particularly high DSi concentrations that were measured in the fjords of northern Chilean Patagonia (Torres *et al.*, 2014) originate from the weathering of Holocene volcanic material, which is exceptionally abundant in northern Chilean Patagonia, and the subsequent transport of dissolved material by river systems. Calculations based on trends in SiO_2 concentrations in profiles AP12-04, AP12-02, and AP13-11 and on average volcanic ash soil thickness result in an estimated value of 2.43 $\times 10^9$ tons of silica leached from the five studied watersheds since the deglaciation. Comparison with present-day river discharge and DSi concentrations suggests that DSi concentrations in north Patagonian rivers were similar to present-day values during most of the Holocene, i.e. since the start of volcanic ash deposition. Without volcanic ash soils, lake and fjord primary productivity in Chilean Patagonia would likely be significantly reduced, resulting in lower rates of carbon burial.

Conclusions

Volcanic ash soils cover a vast area of northern Chilean Patagonia (44–48°S). According to the isopach map created in this study, their distribution is significantly influenced by the Westerlies, with thick andosols occurring on large distances to the east of the regional volcanoes. Their western extent, on the other hand, is restricted to a few tens of kilometers from the source volcanoes. Down-profile variations in mineralogy and geochemistry indicate that the andosols are heavily weathered, and that weathering releases significant amounts of dissolved silica to the regional rivers, mostly through leaching from volcanic glass. At the regional scale, a highly positive correlation was found between average andosol thickness and riverine DSi concentrations, suggesting that andosol thickness is the main parameter that affects spatial variations in DSi concentrations in north Patagonian river systems. Although glacier coverage also significantly correlates with riverine

DSi concentrations, the influence of glaciers on river chemistry is not independent of ash soil distribution, and it mostly affects variations in DSi at seasonal timescales. Our results therefore show that andosol weathering is the main source of DSi to the rivers, lakes, and fjords of northern Chilean Patagonia. The presence of a thick cover of volcanic ash soils in the region helps explain the particularly high rates of biogenic productivity that were measured in the regional fjords. In addition, our results suggest that terrestrial weathering may strengthen the efficacy of the biological pump, and therefore increase the drawdown of atmospheric CO_2 concentrations, even at millennial timescales.

Acknowledgements—The mineralogical and geochemical data presented in this paper are available on Earthchem (DOI: 10.1594/IEDA/100526). This research was supported by FWO Research Grant 1.5.104.11N to S. Bertrand. We are grateful to Zakaria Ghazoui (UJF Grenoble, France), Jean-Yves De Vleeschouwer (ULg-Gembloux, Belgium), Francois De Vleeschouwer (Ecolab, Toulouse, France), Alberto Araneda (EULA, Concepción, Chile), and Olaf Wundrich and Jammie Valdivia (ColibriVentura, Coyhaique, Chile) for their support during the field expeditions. The Chilean Dirección General de Aguas (DGA) provided the river discharge and meteorological data presented in Figures S2, S3, and S4. Diego Caamaño (UCSC, Concepción, Chile) provided the ADCP that was used to measure river discharge. N. Fagel and J. Otten (Department of Geology, ULg) are thanked for their assistance during XRD analyses. N. Delmelle is thanked for preparing the samples for XRF analyses. E. Van Ranst and V. Galy are thanked for the DSi measurements and for providing the filtration system, respectively. Samples were collected with authorization from CONAF, SHOA (13270/24/693/VRS), and DIFROL (282, 330, and 434). Two anonymous reviewers are acknowledged for providing constructive remarks on an earlier version of this article. This research was conducted while S. Bertrand was a postdoctoral fellow of the Flemish Research Foundation (FWO, Belgium). B. Reid's participation was funded by FONDECYT project 11110293 and by a CONICYT seed grant. E. Vandekerkhove is currently supported by FWO project G042812N (to M. De Batist).

References

Andrews JE, Brimblecombe P, Jickells TD, Liss PS, Reid BJ. 2004. The chemistry of continental solids. In *An Introduction to Environmental Chemistry*. Blackwell Publishing: Oxford, UK; 97–99.

Aracena C, Lange CB, Luis Iriarte J, Rebolledo L, Pantoja S. 2011. Latitudinal patterns of export production recorded in surface sediments of the Chilean Patagonian fjords (41–55°S) as a response to water column productivity. *Continental Shelf Research* **31**: 340–355. DOI:10.1016/j.csr.2010.08.008.

Arnalds O. 2012. Andosols. In *Encyclopedia of Soil Science*, Chesworth W (ed). Springer: Berlin.

Bartels A. 2012. Aard en verspreiding van vulkanische bodems in Noord-Patagonië, Chili. Master thesis, Universiteit Gent; 103.

Bertrand S, Fagel N. 2008. Nature, origin, transport and deposition of andosol parent material in south-central Chile (36–42°S). *Catena* **73**: 10–22. DOI:10.1016/j.catena.2007.08.003.

Bertrand S, Hughen KA, Sepúlveda J, Pantoja S. 2012. Geochemistry of surface sediments from the fjords of Northern Chilean Patagonia (44–47°S): spatial variability and implications for paleoclimate reconstructions. *Geochimica et Cosmochimica Acta* **76**: 125–146. DOI:10.1016/j.gca.2011.10.028.

Bertrand S, Daga R, Bedert R, Fontijn K. 2014. Deposition of the 2011 Puyehue-Cordon de Caulle tephra (Chile, 40°S) in lake sediments: implications for tephrochronology and volcanology. *Journal of Geophysical Research, Earth Surface* **119**: 2555–2573. DOI:10.1002/2014JF003321.

Brown G, Brindley GW. 1980. X-ray diffraction procedures for clay mineral identification. In *Crystal Structures of Clay Minerals and X-ray Identification*, Brown G, Brindley GW (eds). Mineralogical Society: London; 305–360.

Calvete C, Sobarzo M. 2011. Quantification of the surface brackish water layer and frontal zones in southern Chilean fjords between Boca del Guafo (43°30′S) and Estero Elefantes (46°30′S). *Continental Shelf Research* **31**: 162–171. DOI:10.1016/j.csr.2010.09.013.

Cas R, Wright JV. 1995. *Volcanic Successions: Modern and Ancient*. Chapman and Hall: London.

Cembrano J, Lara L. 2009. The link between volcanism and tectonics in the southern volcanic zone of the Chilean Andes: a review. *Tectonophysics* **471**: 96–113. DOI:10.1016/j.tecto.2009.02.038.

Conley DJ, Stalnacke P, Pitkanen H, Wilander A. 2000. The transport and retention of dissolved silicate by rivers in Sweden and Finland. *Limnology and Oceanography* **45**: 1850–1853. DOI:10.4319/lo.2000.45.8.1850.

Cook HE, Johnson PD, Matti JC, Zemmels I. 1975. Methods of sample preparation and X-ray diffraction data analysis, X-ray mineralogy laboratory, deep sea drilling project, University of California, Riverside. In *Initial Reports of the Deep Sea Drilling Project*, Hayes DE, Frayes LA (eds). US Government Printing Office: Washington; 999–1007.

De Los Ríos-Escalante P, Quinán E, Acevedo P. 2013. Crustacean zooplankton communities in Lake General Carrera (46°S) and their possible association with optical properties. *Crustaceana* **86**: 507–513. DOI:10.1163/15685403-00003182.

Domic Kuscevic L, Fuentes Aravana A, Gecele CP. 2000. *Geografía de Chile*. Santillana del Pacífico SA: Santiago, Chile.

D'Orazio M, Innocenti F, Manetti P, Tamponi M, Tonarini S, Gonzalez-Ferran O, Lahsen A, Omarini R. 2003. The Quaternary calc-alkaline volcanism of the Patagonian Andes close to the Chile triple junction: geochemistry and petrogenesis of volcanic rocks from the Cay and Maca volcanoes (~45°S, Chile). *Journal of South American Earth Sciences* **16**: 219–242. DOI:10.1016/S0895-9811(03)00063-4.

Duffield WA, Bacon CR, Roquemore GR. 1979. Origin of reverse-graded bedding in air-fall pumice, Coso Range, California. *Journal of Volcanology and Geothermal Research* **5**: 35–48. DOI:10.1016/0377-0273(79)90031-3.

Dussaillant A, Buytaert W, Meier C, Espinoza F. 2012. Hydrological regime of remote catchments with extreme gradients under accelerated change: the Baker basin in Patagonia. *Hydrological Sciences Journal* **57**: 1530–1542. DOI:10.1080/02626667.2012.726993.

Fontijn K, Lachowycz SM, Rawson H, Pyle DM, Mather TA, Naranjo JA, Moreno-Roa H. 2014. Late quaternary tephrostratigraphy of southern Chile and Argentina. *Quaternary Science Reviews* **89**: 70–84. DOI:10.1016/j.quascirev.2014.02.007.

Fuenzalida R. 1974. The Hudson volcano. Proceedings of the Symposium on Andean and Antarctic Volcanology Problems, Santiago, Chile, September 1974; 78–87.

Futa K, Stern CR. 1988. Sr and Nd isotopic and trace-element compositions of quaternary volcanic centers of the southern Andes. *Earth and Planetary Science Letters* **88**: 253–262. DOI:10.1016/0012-821x(88)90082-9.

Garreaud RD, Vuille M, Compagnucci R, Marengo J. 2009. Present-day South American climate. *Palaeogeography Palaeoclimatology Palaeoecology* **281**: 180–195.

Garreaud R, Lopez P, Minvielle M, Rojas M. 2013. Large-scale control on the Patagonian climate. *Journal of Climate* **26**: 215–230. DOI:10.1175/Jcli-D-12-00001.1.

Gerlach DC, Frey FA, Morenoroa H, Lopez-Escobar L. 1988. Recent volcanism in the Puyehue Cordon-Caulle region, Southern-Andes, Chile (40.5°S): petrogenesis of evolved lavas. *Journal of Petrology* **29**: 333–382.

Glasser NF, Harrison S, Jansson KN, Anderson K, Cowley A. 2011. Global sea-level contribution from the Patagonian Icefields since the Little Ice Age maximum. *Nature Geoscience* **4**: 303–307. DOI:10.1038/NGEO1122.

Glasser NF, Harrison S, Schnabel C, Fabel D, Jansson KN. 2012. Younger Dryas and early Holocene age glacier advances in Patagonia. *Quaternary Science Reviews* **58**: 7–17. DOI:10.1016/j.quascirev.2012.10.011.

Grez RZ. 1984. Characteristicas de suelos del litoral de Aysen, Sector Canal Costa, Fiordo quitralco y Golfo Elefantes. *Boletín Sociedad Chilena de la Ciencia del Suelo* **4**: 65–75.

Gut B. 2008. Geology, climate, and soils of Patagonia. In *Trees in Patagonia*. Springer: Basel; 9–18.

Haberle SG, Lumley SH. 1998. Age and origin of tephras recorded in postglacial lake sediments to the west of the southern Andes, 44°S to 47°S.

Journal of Volcanology and Geothermal Research **84**: 239–256. DOI:10.1016/S0377-0273(98)00037-7.

Hervé F, Pankhurst RJ, Drake R, Beck M. 1995. Pillow metabasalts in a mid-tertiary extensional basin adjacent to the Liquiñe-Ofqui fault zone: the Isla Madgalena area, Aysén, Chile. *Journal of South American Earth Sciences* **8**: 33–46. DOI:10.1016/0895-9811(94)00039-5.

Hickey RL, Frey FA, Gerlach DC, Lopezescobar L. 1986. Multiple sources for basaltic arc rocks from the Southern Volcanic zone of the Andes (34°S–41°S): trace-element and isotopic evidence for contributions from subducted oceanic-crust, mantle, and continental-crust. *Journal of Geophysical Research: Solid Earth and Planets* **91**: 5963–5983. DOI:10.1029/Jb091ib06p05963.

Hickey-Vargas R, Gerlach D, Frey F. 1984. Geochemical variations in volcanic rocks from central-south Chile (33°–41°S): implications for their petrogenesis. In *Andean Magmatism: Chemical and Isotopic Constraints*, Harmon R, Barreiro B (eds). Shiva: NantwichF; 72–95.

Hickey-Vargas R, Moreno H, López-Escobar L, Frey F. 1989. Geochemical variations in Andean basaltic and silicic lavas from the Villarrica-Lanín volcanic chain (39.5°S): an evaluation of source heterogeneity, fractional crystallization and crustal assimilation. *Contributions to Mineralogy and Petrology*: 361–386.

Hijmans RJ, Cameron SE, Parra JL, Jones PG, Jarvis A. 2005. Very high resolution interpolated climate surfaces for global land areas. *International Journal of Climatology* **25**: 1965–1978. DOI:10.1002/Joc.1276.

Hulton NRJ, Purves RS, McCulloch RD, Sugden DE, Bentley MJ. 2002. The last glacial maximum and deglaciation in southern south America. *Quaternary Science Reviews* **21**: 233–241. DOI:10.1016/S0277-3791(01)00103-2.

JGOFS, 1996. Protocols for the JGOFS core measurements. JGOFS Report Nr. 19.

Laugenie C. 1982. *La région des lacs, Chili méridional*. Université de Bordeaux III: France.

López-Escobar L, Frey F, Vergara M. 1977. Andesites and high-alumina basalts from the central-south Chile high Andes: geochemical evidences bearing on their petrogenesis. *Contributions to Mineralogy and Petrology* **63**: 199–228.

López-Escobar L, Killian R, Kempton P, Tagiri M. 1993. Petrography and geochemistry of Quaternary rocks from the Southern Volcanic Zone between 41°30′ and 46°00′S, Chile. *Revista Geologica De Chile* **20**(1): 35–55.

López-Escobar L, Cembrano J, Moreno H. 1995. Geochemistry and tectonics of the Chilean Southern Andes basaltic quaternary volcanism (37–46°S). *Revista Geologica De Chile* **22**: 219–234.

Luebert F, Pliscoff P. 2006. *Sinopsis bioclimática y vegetacional de Chile*. Editorial Universitaria: Santiago.

Markgraf V, Whitlock C, Haberle S. 2007. Vegetation and fire history during the last 18 000 cal yr BP in Southern Patagonia: Mallin Pollux, Coyhaique, Province Aisen (45°41′30″ S, 71°50′30″ W, 640 m elevation). *Palaeogeography Palaeoclimatology Palaeoecology* **254**: 492–507. DOI:10.1016/j.palaeo.2007.07.008.

McCurdy BS. 2003. *Geochemistry and clay mineralogy of volcanic paleosols from Chile's Tenth region: implications for use of andic soils in paleoclimate interpretations, trace metal stability and geochemical fingerprints*. Middlebury College: Vermont, USA.

Miller A. 1976. The climate of Chile. In *Climates of Central and South America*, Schwerdtfeger W (ed). Elsevier: Amsterdam; 113–145.

Naranjo JA, Stern CR. 1998. Holocene explosive activity of Hudson Volcano, southern Andes. *Bulletin of Volcanology* **59**: 291–306. DOI:10.1007/s004450050193.

Naranjo JA, Stern CR. 2004. Holocene tephrochronology of the southernmost part (42°30′–45° S) of the Andean southern volcanic zone. *Revista Geologica De Chile* **31**: 225–240. DOI:10.4067/S0716-02082004000200003.

Nelson E, Bruce E, Elthon D, Kammer D, Weaver S. 1988. Regional lithologic variation in the Patagonian batholiths. *Journal of South American Earth Sciences* **1**: 239–247.

Nelson DM, Treguer P, Brzezinski MA, Leynaert A, Queguiner B. 1995. Production and dissolution of biogenic silica in the ocean - revised global estimates, comparison with regional data and relationship to biogenic sedimentation. *Global Biogeochemical Cycles* **9**: 359–372. DOI:10.1029/95gb01070.

Nesbitt HW, Young GM. 1982. Early proterozoic climates and plate motions inferred from major element chemistry of lutites. *Nature* **299**: 715–717.

Pankhurst RJ, Weaver SD, Herve F, Larrondo P. 1999. Mesozoic-Cenozoic evolution of the North Patagonian Batholith in Aysen, southern Chile. *Journal of the Geological Society* **156**: 673–694. DOI:10.1144/gsjgs.156.4.0673.

Peri PL, Bloomberg M. 2002. Windbreaks in southern Patagonia, Argentina: a review of research on growth models, windspeed reduction, and effects on crops. *Agroforestry Systems* **56**: 129–144. DOI:10.1023/A:1021314927209.

Pfeiffer M, Mascayano C, Aburto F. 2010. Soils of Chilean Patafonia in glacial and periglacial environments. *Eurasian Soil Science* **43**: 1430–1438. DOI:10.1134/S106422931013003X.

de Porras ME, Maldonado A, Abarzúa AM, Cáardenas ML, Francois JP, Martel-Cea A, Stern CR, Méndez C, Reyes O. 2012. Postglacial vegetation, fire and climate dynamics at Central Chilean Patagonia (Lake Shaman, 44°S). *Quaternary Science Reviews* **50**: 71–85. DOI:10.1016/j.quascirev.2012.06.015.

de Porras ME, Maldonado A, Quintana FA, Martel-Cea A, Reyes O, Méndez C. 2014. Environmental and climatic changes in Central Chilean Patagonia since the Late Glacial (Mallín El Embudo, 44°S). *Climate of the Past* **10**: 1–16. DOI:10.5194/cp-10-1-2014.

Ruggieri F, Fernández-Turiel J-L, Saavedra J, Gimeno D, Polanco E, Naranjo JA. 2011. Environmental geochemistry of recent volcanic ashes from the Southern Andes. *Environmental Chemistry* **8**: 236–247.

Sagredo EA, Lowell TV. 2012. Climatology of Andean glaciers: a framework to understand glacier response to climate change. *Global and Planetary Change* **86–87**: 101–109. DOI:10.1016/j.gloplacha.2012.02.010.

Segemar. 1998. Mapa geologico de la Republica Argentina, scale 1/2.500.000.

Sepúlveda J, Pantoja S, Hughen KA. 2011. Sources and distribution of organic matter in northern Patagonia fjords, Chile (~44–47°S): a multi-tracer approach for carbon cycling assessment. *Continental Shelf Research* **31**: 315–329. DOI:10.1016/j.csr.2010.05.013.

Sernageomin. 2003. Mapa geologico de Chile version digital, scale 1/1.000.000.

Shoji S, Nanzyno M, Dahlgren RA. 1993. *Volcanic Ash Soils: Genesis. Properties and Utilization*. Elsevier Science Publishers B.V.: Amsterdam, The Netherlands.

Smith RW, Bianchi TS, Allison M, Savage C, Galy V. 2015. High rates of organic carbon burial in fjord sediments globally. *Nature Geoscience* **8**: 450–453. DOI:10.1038/NGEO2421.

Stern CR, Moreno H, López-Escobar L, Clavero JE, Lara LE, Naranjo JA, Parada MA, Skewes MA. 2007. Chilean volcanoes. In *The Geology of Chile*, Moreno T, Gibbons W (eds). The Geological Society: London; 147–178.

Stern CR, de Porras ME, Maldonado A. 2015. Tephrochronology of the upper Río Cisnes valley (44°S), southern Chile. *Andean Geology* **42**: 173–189. DOI:10.5027/andgeoV42n2-a02.

Strickland JDH, Parsons TR. 1968. Determination of reactive silicate. In *A Practical Handbook of Seawater Analysis*. Fisheries Research Board of Canada: Ottawa; 65–70.

Torres R, Silva N, Reid B, Frangopulos M. 2014. Silicic acid enrichment of subantarctic surface water from continental inputs along the Patagonian archipelago interior sea (41–56°S). *Progress in Oceanography* **129**: 50–61. DOI:10.1016/j.pocean.2014.09.008.

Turner KJ, Fogwill CJ, McCulloch RD, Sugden DE. 2005. Deglaciation of the eastern flank of the North Patagonian Icefield and associated continental-scale lake diversions. *Geografiska Annaler Series a-Physical Geography* **87A**: 363–374. DOI:10.1111/j.0435-3676.2005.00263.x.

Van Daele M, Bertrand S, Meyer I, Moernaut J, Vandoorne W, Siani G, Tanghe N, Ghazoui Z, Pino M, Urrutia R & De Batist M. 2016. —Late Quaternary evolution of Lago Castor (Chile, 45.6°S): Timing of the deglaciation in northern Patagonia and evolution of the southern westerlies during the last 17kyr. *Quaternary Science Reviews* **133**: 130–146.

Villa-Martinez R, Moreno PI. 2007. Pollen evidence for variations in the southern margin of the westerly winds in SW Patagonia over the last 12,600 years. *Quaternary Research* **68**: 400–409. DOI:10.1016/j.yqres.2007.07.003.

Villa-Martínez R, Moreno PI, Valenzuela MA. 2012. Deglacial and postglacial vegetation changes on the eastern slopes of the central Patagonian Andes (47°S). *Quaternary Science Reviews* **32**: 86–99. DOI:10.1016/j.quascirev.2011.11.008.

Weller D, Miranda CG, Moreno PI, Villa-Martinez R, Stern CR. 2014. The large late-glacial Ho eruption of the Hudson volcano, southern Chile. *Bulletin of Volcanology* **76**. DOI:10.1007/S00445-014-0831-9.

Wilson TM, Cole JW, Stewart C, Cronin SJ, Johnston DM. 2011. Ash storms: impacts of wind-remobilised volcanic ash on rural communities and agriculture following the 1991 Hudson eruption, southern Patagonia, Chile. *Bulletin of Volcanology* **73**: 223–239. DOI:10.1007/s00445-010-0396-1.

Wolff-Boenisch D, Gislason SR, Oelkers EH, Putnis CV. 2004. The dissolution rates of natural glasses as a function of their composition at pH 4 and 10.6, and temperatures from 25 to 74 °C. *Geochimica et Cosmochimica Acta* **68**: 4843–4858. DOI:10.1016/j.gca.2004.05.027.

Wright JV, Smith AL, Self S. 1980. A working terminology of pyroclastic deposits. *Journal of Volcanology and Geothermal Research* **8**: 315–336.

Supporting Information

Additional supporting information may be found in the online version of this article at the publisher's web-site.